ACS APPLIED MATERIALS & INTERFACES

Research Article

www.acsami.org

Simple Strategy for Producing Superhydrophobic Nanocomposite Coatings In Situ on a Building Substrate

Dario S. Facio and Maria J. Mosquera*

TEP-243 Nanomaterials Group, Departamento de Química-Física, Facultad de Ciencias, Campus Universitario Río San Pedro, Universidad de Cádiz, 11510 Puerto Real, Cádiz, Spain

Supporting Information

ABSTRACT: Numerous superhydrophobic materials have been developed in recent years by using a combination of two strategies: reducing the surface free energy and roughening the surface. Most of these procedures have the serious drawback of involving tedious multistage processes, which prevent their large-scale application, such as on the external stone and similar material surfaces of buildings exposed to the weather. This paper describes an innovative synthesis route for producing superhydrophobic surface coatings. The coating can even be produced, outdoors, on the building by a low-cost process. We demonstrate that the addition of silica nanoparticles to a mixture of organic and inorganic silica oligomers in the presence of a surfactant produces a coating of closely packed particles. The effect of this is to trap air beneath the water droplets, thus significantly minimizing the contact area between droplet and surface. The organic component reduces the surface free energy of the material, resulting in a high static contact angle. This has the effect of repelling water because the water droplets that form simply roll rapidly down the coated surface. The surfactant plays a valuable role, acting as a sol−gel transition catalyst and, by coarsening the pore structure of the gel network, prevents the coating material from cracking.

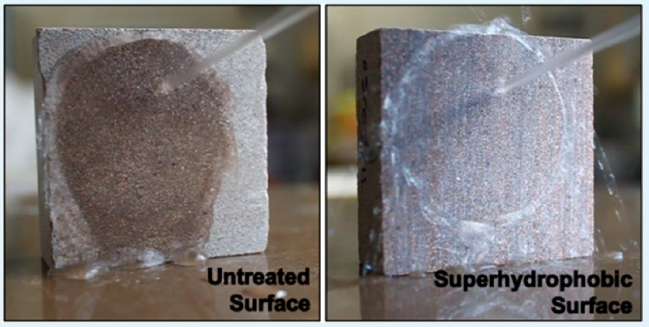

KEYWORDS: *superhydrophobic surfaces, nanocomposite, building materials, close-packed coating, surfactant directing-agent*

INTRODUCTION

In recent years, superhydrophobic surface coatings have attracted considerable attention because of their numerous claimed properties, such as biomimicking, antiadhesion, contamination prevention, water repellent abilities, and self-cleaning capacities.[1,2] The requirements of these coated surfaces are to generate a water contact angle greater than 150° and a low contact angle hysteresis, below 10°. This last requirement is important because, as Gao and McCarthy[3] emphasize, the contact angle hysteresis (the difference between the receding and the advancing contact angles) controls water droplet movement (i.e., the water repellent effect).

Because the contact angle on smooth hydrophobic surfaces does not exceed 120°, it is assumed that superhydrophobic surfaces can be achieved by combining two strategies: reducing the surface free energy and roughening the surface. It is confirmed by the superhydrophobicity observed on the leaves of the lotus and other plants. It is widely recognized that this phenomena is due to the special micronano-binary structure of the lotus leaves, which increases the surface roughness and minimizes the contact area between the leaf and the liquid. The effect of this roughness is that a layer of air is trapped beneath the water droplet, thus assisting the water droplets to roll off the surface.[4]

Inspired by these natural structures, numerous superhydrophobic surfaces have been produced by means of a variety of techniques including etching and lithography,[5,6] self-assembly and sol−gel processing,[7,8] generally followed by further chemical modification. The drawback of these procedures is that they involve tedious and multistage processes, which prevent their large-scale application, particularly on exposed surfaces of buildings and structures.

Specifically, the application on buildings is very restrictive because the product has to be applied under outdoors conditions. Moreover, any operation additional, such as heating or solvent extraction, is extremely difficult and expensive. However, several trials for producing various superhydrophobic products for application to building materials, such as stonework, have been described in the literature. The research group of Karapanagiotis[9,10] has produced polymer−particle composite films that have superhydrophobic properties when applied on surfaces of stone and other building materials, such as glass or wood. Those films were created by spraying metal oxide nanoparticles dispersed in polymer (siloxane or acrylic) on the building substrate. Polymer is dissolved in volatile organic solvents (VOCs), and annealing treatment under vacuum is applied to remove the residual solvent. Recently, de Ferri et al.[11] have obtained superhydrophobic products that can

Received: May 15, 2013
Accepted: July 15, 2013
Published: July 15, 2013

   dx.doi.org/10.1021/am401826g | ACS Appl. Mater. Interfaces 2013, 5, 7517−7526

be applied to stonework, by mixing alkoxysilanes and modified silica particles. These materials were synthesized by a classic sol−gel route using HCl as a catalyst and EtOH as a solvent. However, their main disadvantage is associated with the cracking of the films and a significant reduction of the hydrophobicity when the treated stones are exposed to water for long periods.Our research group has recently designed several products for restoring and protecting building materials. Specifically, we have prepared consolidant products,[12,13] hydrophobic materials,[13−15] and photoactive products with self-cleaning properties.[16−19] No heating process is required in any of the synthesis processes developed in our laboratory. Thus, our products are very suitable for application on thermally sensitive substrates; they are produced by a low-cost process; and, of especial relevance, they meet the operational and commercial requirements for application to exterior surfaces of large buildings and structures. The process is so simple that the coatings are produced on the exposed surfaces requiring treatment, under outdoor conditions, using very common deposition methods, such as brushing or spraying. Some of these products are available as commercial products under the corresponding exploitation patents.[20−22]

This previous research represented the starting point for the development of a one-step synthesis of low cost to produce superhydrophobic coatings for exposed surfaces of buildings and other structures. Our hypothesis proposes that silica nanoparticles mixed with a silica oligomer and a low-molecular-weight organic siloxane in presence of a surfactant should produce an effective coating product. The organic component should reduce the surface energy, thus giving the surface a valuable hydrophobic property, and the nanoparticles should create a surface roughness that will enhance the hydrophobicity produced. There are two fundamental reasons for adding a surfactant (such as *n*-octylamine) to our sol: (1) to coarse the pore structure of the gel network, preventing cracking when the product dries;[12,13] and (2) to act as a basic catalyst of the sol transition on the substrate surface.[13,16] Finally, it is significant that no volatile organic compound (VOC) is added to the sol. The volatile organic solvents are removed by two reasons: (1) to produce "green" products, and (2) to enhance the products dry matter in order to increase their effectiveness.[13] With the procedure proposed, there is no need for any annealing treatment or other action for the removal of solvent after the application of the coating.

The paper is organized as follows: First, we report about the synthesis process developed in our laboratory and the means used for the characterization of the product obtained. To evaluate the effect of silica particles on the final properties of the material, we have prepared a gel without particles according to the same procedure. Second, the two products have been applied to the surface of a stone commonly used as building material; and their effectiveness for hydrophobic purposes has been evaluated. For comparison, a commercial hydrophobic product was also evaluated. Specifically, an in-depth investigation of the structure of the synthesized material has been made in order to establish the relationship between its superhydrophobic property and its nanostructure.

EXPERIMENTAL SECTION

Synthesis. Silica nanocomposites were prepared by mixing TES 40 WN, obtained from Wacker (hereafter TES40), a hydroxyl-terminated polydimethylsiloxane, obtained from ABCR (hereafter PDMS), and AEROSIL OX50 colloidal silica particles, obtained from Evonik (hereafter OX50), in the presence of a surfactant (*n*-octylamine, obtained from Aldrich). According to its technical data sheet, TES40 is a mixture of monomeric and oligomeric ethoxysilanes, with an average chain length of approximately 5 Si−O units. PDMS has a polymerization degree of 12 with a molecular mass between 400 and 700, and an OH percentage ranging from 4 to 6% w/w. OX50 is hydrophilic fumed silica with a particle diameter of 40 nm.

The starting sol was prepared according the following procedure: (1) a 1.57 M aqueous solution of *n*-octylamine was prepared, being the concentration of the surfactant significantly higher than that corresponding to its critical micellar concentration (cmc), which is 0.010 M.[23] (2) TES40, OX50, and the aqueous solution of *n*-octylamine were mixed under ultrasonic stirring (60 W cm^{-3}). (3) PDMS was further added dropwise to the mixture maintaining the stirring for an additional 10 min. For comparative purposes, we also prepared a hybrid nanomaterial in a similar way, but excluding the addition of silica colloidal particles (OX50). The composition of the sols under study is given in Table 1 and an illustration of the synthesis process is presented in Scheme 1. The products were named UCA (after the University of Cadiz) followed by T (initial letter of TES40) and P (initial letter of PDMS). The letter S (silica particles) was included in the formulation containing these particles.

Table 1. Compositions of Sols under Study

product	TES40 (%v/v)	PDMS (%v/v)	surfactant solution (%v/v)	OX50 (%w/v)
UCA-TP	89.40	10.45	0.15	
UCA-TPS	89.40	10.45	0.15	5

Scheme 1. Synthesis Route and Application Developed in This Work

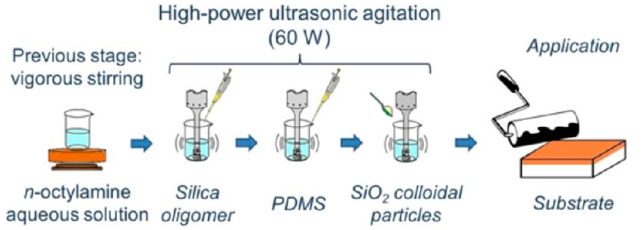

Characterization of Nanomaterials. Immediately after the synthesis, the rheological properties of the sols were studied using a concentric cylinder viscosimeter (model DV-II+ with UL/Y adapter) from Brookfield. Experiments were performed at 25 °C maintained by the recirculated water from a thermostatic bath. For comparative purposes, the viscosity of a commercial product, Silres BS290 supplied by Wacker (hereafter BS290) was also evaluated. BS290 is a solvent-free silane/siloxane mixture with application as hydrophobic treatment. Following the specifications of the manufacturer, BS290 was diluted in ethanol (dilution: 12% w/w).

Next, the sols were cast, without being covered, in cylindrical and transparent molds of diameter 3.2 cm, adding 2 mL per cast. The sols were cast in open vessels in order to simulate the sol−gel transition that take place on the substrate. The cast sols were kept under laboratory conditions (60% RH and 20 °C). Gel transition took place spontaneously and the gel time was recorded. The stability of the sols was also evaluated by measuring the gel time in the enclosed condition. Gels were left to dry until a constant weight was reached. The presence of cracks in the xerogels was checked by visual inspection. Finally, all the experiments described in the next paragraph were carried out six months after the synthesis.

The contraction in volume of the materials during drying was calculated from the volume change undergone by the xerogel monoliths, using a digital calliper from Comecta.

Fourier transformer infrared spectra (FTIR) were recorded in the surface of the xerogels using a FTIR-8400S from Shimadzu (4 cm^{-1} in resolution) in the region from 4000 to 650 cm^{-1}. Experiments were carried out in attenuated total reflection mode (ATR).

Energy-dispersive X-ray spectroscopy (EDX) was determined on the surface of the xerogels prepared in our laboratory using a JEOL Quanta 200 scanning electron microscope (SEM).

Textural characterization was carried out by N_2 physisorption at 77 K, using an Autosorb IQ from Quantachrome. The isotherms obtained were used to calculate pore volume, pore size distribution and BET surface area of the powdered xerogels.

Transmission electron microscopy studies were performed using a JEOL 2010F TEM/STEM microscope, equipped with a JEOL high angle annular dark field (HAADF) detector, enabling the acquisition of STEM images. Details of the procedure are given in a previous paper.[17]

Dynamic light scattering (DLS) experiments were carried out on a Malvern Zetasizer Nano S instrument, using a 4mW He−Ne laser operating at a wavelength of 632.8 nm and an avalanche photodiode (APD) detector at 90°.

Application on Stone Surface and Characterization. Products under study were applied onto a common building stone. The stone selected is a sandstone with porosity of around 4.5%. It is composed of quartz (60%), feldspar (25%) and phyllosilicates (10%) and low content of calcite. Sols under study were applied by brushing with a paint roller on the upper surface of 5 × 5 × 2 cm cube samples. In order to prevent water uptake through the sides of the cube in the capillary water absorption test, the sol was also applied on the sides of the samples, as shown in Scheme 1. Immediately after the application, products uptake was calculated. Next, the stone samples were then dried under laboratory conditions until constant weight was reached. The untreated stone samples and their treated counterparts were subjected to the characterization process described in the following paragraphs. The characterization was carried out six months after the application. First, product dry matter was calculated. Second, the samples corresponding to untreated stone and their treated counterparts were characterized by the procedures described below. All the results reported correspond to average values obtained from three stone samples.

The hydrophobic behavior of the coating materials was determined by water contact angle test (sessile drop method), using a commercial video-based, software-controlled contact angle analyzer, model OCA 15plus, from Dataphysics Instruments. Static and dynamic (advancing and receding) contact angle values were determined according to the procedure previously reported.[14]

To confirm the hydrophobic and repellence properties of the coating produced in our laboratory, the following tests were carried out.

To test the adhesion of a water droplet on the treated stone surface, we performed the following experiment using the commercial video-based contact angle analyzer described in the previous paragraph: sessile water droplets (10 μL) were deposited from a needle on stone surfaces covered with the UCA products under study and on their untreated counterpart. Next, the stone samples were moved from left to right in order to test if the droplet adheres to the surface.

To test repellence properties, we deposited several water droplets on a treated stone surface. Next, the sample was slightly tilted. It was recorded by a digital compact camera (Sony Cyber-Shot model DSC-P200) at 30 frames/s.

The treated stone surface and its untreated counterpart were soaked by holding them under running cold water from a normal tap, in order to visualize if the water penetrated into the stones. The experiment was recorded by the same camera described in the previous paragraph.

Finally, the stone samples were subjected to a test of water absorption by capillarity (WAC) as recommended in UNE-EN 1925.[24]

Scanning electron microscopy was used to visualize changes in the morphology of the stone after the treatments. The microscope employed was a model Sirion FEG SEM from the FEI Company. Details of the experimental procedure are given in a previous paper.[13]

The topography of the surface of the stone after coating with the products under study and its untreated counterpart was observed using atomic force microscopy (AM-AFM, Nanotec Electrónica S.L.) operated in tapping mode. The root-mean-square (RMS) roughness values were calculated from 2.5 μm × 2.5 μm images.

We also evaluated the possible disadvantage of these materials associated with changes in stone color induced by the treatments. Total color difference (ΔE^*) was determined using a solid reflection spectrophotometer, Colorflex model, from Hunterlab. The conditions used were: illuminant C and observer CIE 10°. CIE L*a*b* scale was used, and variations in color were evaluated.[25]

Finally, we measured the penetration depth of the products under study. Images of the cross-sections of the treated stones and their untreated counterparts were obtained using a Nikon model SMZ800 stereoscopic microscope, according to the following procedure: first the stone samples were immersed in water; next, they were cut and visualized by microscopy. The nonwetted area can be associated with the penetration depth of the products across the pore structure of the stone samples.

RESULTS AND DISCUSSION

Characterization of Materials. The sol−gel properties of these materials are shown in Table 2. The sols under study exhibited a Newtonian behavior at the shear range evaluated (the linear regression coefficients were above 0.99). Therefore, the viscosity was calculated as the slope of the shear rate vs shear stress curve. The commercial hydrophobic product (BS290) showed the lowest viscosity value as a consequence of its dilution in ethanol. The two sols prepared in our laboratory showed a similar viscosity, being slightly higher for the nanocomposite due to the effect of silica particles (see Table 2).

Table 2. Sol−Gel Properties

product	viscosity (m Pa s)	gel t^a (days)	stability (months)	vol. reduction (%)
BS290	3.13		12[b]	
UCA-TP	5.35	3	8	49
UCA-TPS	6.54	3	7	36

[a]Gel t is gel time. [b]According to the manufacturers specifications.

Regarding the gel times observed in open vessels, which simulate the sol−gel transition that takes place on the substrate, both UCA products gel spontaneously under laboratory conditions, as required. It is also important to point out that the UCA sols showed a long period of stability when they were stored in closed vessels (Table 2).

This demonstrates that our products meet the practical and commercial requirement of retaining their properties during storage for considerable lengths of time prior to their application onto substrates. After drying under laboratory conditions, the two sols synthesized in our laboratory produced homogeneous, crack-free, and transparent monoliths, as shown in Figure 1. The BS290 alcoholic solution produced a white and

Figure 1. Photographs of the xerogels: (a) UCA-TP and (b) UCA-TPS.

dx.doi.org/10.1021/am401826g | ACS Appl. Mater. Interfaces 2013, 5, 7517−7526

dusty residue, because the solvent evaporated completely. The homogeneity of the two xerogels prepared in our laboratory demonstrates that the PDMS is integrated perfectly into the inorganic silica skeleton; this could, a priori, suggest that co-condensation between PDMS and silica oligomers takes place.[26] In the case of the xerogel containing silica particles, this homogeneity also demonstrates that the particles have been uniformly distributed throughout the silica network. The slight whiteness observed in the composite is associated with the nanoparticles added.

With respect to the reduction in volume undergone by the xerogels during the drying phase, the xerogels contraction was significantly less than those produced on our previously synthesized products with a high content of water and ethanol.[14] As we recently discussed,[13] this finding demonstrated that the complete removal of volatile solvents from the synthesis produce a significant increase in the dry matter obtained and, consequently, these products will present a greater effectiveness.

By comparing the volume reduction of the xerogels prepared, we observe that it was lower for the composite containing silica nanoparticles. As previously discussed by Mackenzie et al.,[27] PDMS chains react initially to the stress produced during drying by coiling up. This promotes the reduction in volume of the hybrid material synthesized in our laboratory (UCA-TP). In the case of the composite (UCA-TPS), we think that silica nanoparticles integrated into the silica network complicate the contraction undergone by the PDMS chains and subsequently, the volume reduction is lower.

The chemical bonds in the surface of the xerogels under study were analyzed by FTIR. The spectra obtained are presented in Figure 2. The three spectra analyzed were found to be very similar, corresponding to typical silica gels networks. As expected, the three products contain, moreover, alkyl groups giving hydrophobic properties of the materials under study.[13] By comparing the two products prepared in our laboratory, we observe the spectra were practically equal, suggesting that the surface of the two materials presents the same chemical bonds.

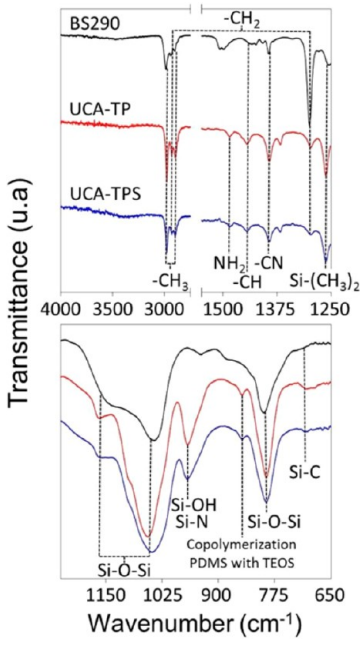

Figure 2. FTIR spectra of the materials under study.

These materials did, however, show some differences with respect to the commercial product: The main difference is the band at 860 cm^{-1} exclusively present in the UCA products and attributed to the co-condensation reaction between silanol groups of hydrolyzed silica oligomers and silanol groups of PDMS molecules. Since the intensity of this peak is not modified as silica nanoparticles are added to the product (UCA-TPS) we think a similar condensation process between OH groups from these particles and those from silica oligomers takes places. In order to confirm the copolymerization, the two UCA materials were exhaustively extracted with ethanol using a Soxhlet apparatus to remove PDMS not bonded to the silica. In both materials the 860 cm^{-1} band is maintained after extraction. This showed that PDMS, and silica nanoparticles added in the case of the UCA-TPS formulation, are covalently bonded to silica particles created during sol−gel transition from the silica oligomer, confirming that the copolymerization process is effective.

Another additional difference is the presence of *n*-octylamine in the UCA xerogels tested. Specifically, the bands are attributed to *n*-octylamine C−N stretching and *n*-octylamine C−H bending, respectively. In addition, we observe a peak at 1485 cm^{-1} which is attributed to amino groups strongly hydrogen-bonded to free silanols. This confirms that the interactions between the surfactant and the oligomer take place by hydrogen bonds and it is not completely removed after air dying, as extensively discussed in a previous paper of our group.[13]

To confirm the identical chemical composition of the two UCA products, we analyzed the surface of these materials by EDX. The results obtained are shown in the Supporting Information (Figure S1). The two materials did not present any difference in their chemical composition. They only show some slight difference in the proportion of the 3 elements detected (Si, C, and O). As expected, the nanocomposite UCA-TPS present a higher proportion of Si and a lower proportion of C element because of the addition of silica nanoparticles to the starting sol induces a slightly lower PDMS content in this formulation.

Textural properties of the xerogels were determined from nitrogen physisorption. The commercial product BS290 was not evaluated because of the low dry matter obtained after drying. The adsorption−desorption isotherms obtained are shown in Figure 3 (top), and the textural data obtained are given in Table 3.

Our xerogels showed typical mesoporous materials isotherms, type IV according to the IUPAC classification. The hysteresis loop was a type H2, characterized by a triangular shape and a steep desorption branch. As previously discussed by Kruk et al.,[28,29] the appearance of a H2 hysteresis loop in the proximity of the lower pressure limit (0.4 for N2 at 77 K) is associated with nanomaterials having uniform cagelike pores, indicating that materials with pores of uniform size have been synthesized.

Figure 3 (bottom) shows the pore size distributions obtained from the data corresponding to desorption branches of the isotherms. The Barret−Joyner−Halenda (BJH) method was employed.[30] The distributions obtained confirm that the UCA materials are composed of a uniform pore size centered on 3.7−4.0 nm, showing a similar distribution. This confirms the role played by the *n*-octylamine as the agent directing the structure of the pores of these materials, as discussed in previous articles of our group.[12−19,26,31] Another kind of

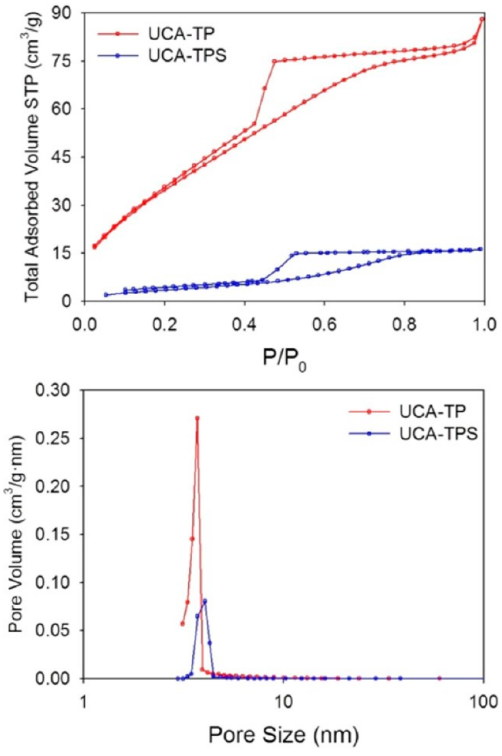

Figure 3. Nitrogen isotherms (top) and BJH pore size distribution (bottom) for the nanomaterials under study.

Table 3. Textural Parameters for the Nanomaterials under Study

product	pore volume (cm^3/g)	pore size (nm)	BET surface area (m^2/g)
UCA-TP	0.14	3.7	145
UCA-TPS	0.03	4.0	15

porosity located at higher pressure (from 0.5 to 1.0), associated with interparticulate spaces inside the gel network,[32] are not observed in these materials. As reported in a previous paper,[13] the absence of these interparticulate spaces in can be interpreted as a consequence of the high shrinkage suffered by PDMS chains during the gel drying phase. By comparing the two UCA materials, we observe that the addition of silica particles, which are a nonporous material, significantly reduces the pore volume and, consequently, the surface area.

For a deeper investigation of the structure of these materials, we carried out a transmission electron microscopy (TEM) study. Figure 4 shows representative images of UCA-TP and UCA-TPS acquired in TEM and HAADF-STEM modes.

The UCA-TP images clearly show that it is composed of a configuration of silica particles of nearly uniform size.[13,26] As previously discussed,[33−35] the formation of these silica particles is produced according to an aggregative growth model in the presence of a basic medium, such as *n*-octylamine, in which the rate of condensation is faster than the hydrolysis.

As commercial OX-50 silica particles are added to the sol in the UCA-TPS product, we observe that a coating composed of particles is also created. However, their size is considerably greater (at around 120 nm). To clarify the discussion, the TEM image corresponding to the commercial particles OX-50 is included in the Supporting Information (Figure S2). As observed, the commercial particles with an initial average size

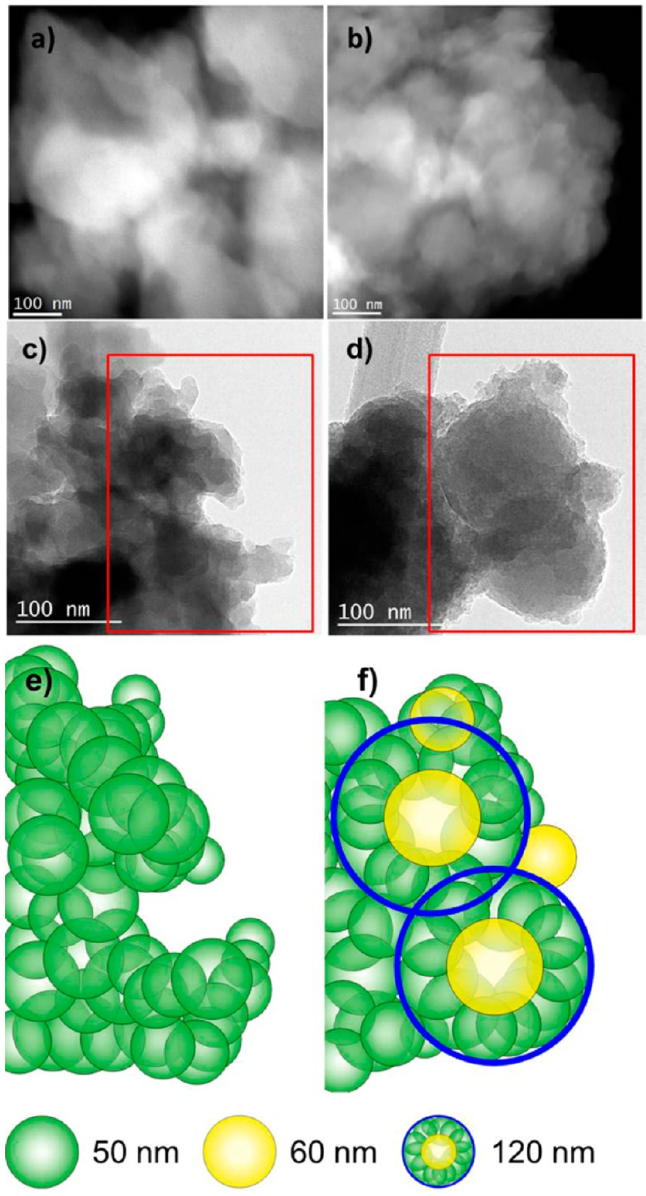

Figure 4. Images of (a, c) UCA-TP and (b, d) UCA-TPS obtained in HAADF-STEM and TEM modes, respectively. Diagrams of the areas included in the marked inset areas for (e) UCA-TP and (f) UCA-TPS are also included. The OX-50 particles added to the starting sol and the silica particles created during sol−gel transition are indicated in yellow and green, respectively.

of 40 nm are aggregated, creating larger particles (of around 80 nm). This finding suggests that the nanocomposite UCA-TPS consists of OX-50 particles aggregated to the silica particles created during sol−gel transition. Thus, this polymer−colloid composite exhibits a significantly higher particle size than its counterpart without OX50 particles.

To confirm the presence of differences in particle size for the two formulations prepared in our laboratory, we investigated the particle size distributions of the UCA starting sols by dynamic light scattering (DLS). The particle size distributions obtained are shown in the Supporting Information (Figure S3). To establish comparisons, we also included the distribution of sizes corresponding to the silica oligomer (TES40). The oligomer histogram presents two perfectly differentiated particle sizes: the smaller size, centered on 2 nm, could

correspond to individual oligomers and the larger size, centered on 150 nm, could be associated with particles corresponding to clusters of oligomers chains. The UCA-TP histogram reveals that the presence of individual oligomers is drastically reduced. Moreover, the clusters size shifts toward the larger value and the histogram becomes narrower. These findings suggest that *n*-octylamine is acting as a catalyst from the moment when the regents are first mixed, because the proportion of clusters and their size are increasing with respect to those corresponding to the oligomer. Obviously, the addition of PDMS also favors the size coarsening because the PDMS chains are slightly longer than that from the TES40.

In the case of the UCA-TPS formulation, we observe a significant shift of the clusters size toward a larger value and a broadening of their distribution. These two features are a consequence of the addition of the silica nanoparticles to the sol. These nanoparticles are aggregated to the gel network as observed previously by TEM, increasing the heterogeneity of the size distribution. Finally, we would state that size of particles measured by TEM and the size obtained by this technique are not comparable for two reasons: (1) we measured the particle size of the xerogels by TEM whereas this parameter was tested in the sol by DLS; (2) we can distinguish individual particles creating an aggregate by TEM, as observed in the Figure 4. However, we only measured the size of the aggregates (clusters). Thus, sizes measured by DLS are significant larger than those obtained by TEM. Finally, we consider that the DLS analysis allows us to confirm that the particle size in UCATPS is higher, even in the starting sol, because of the addition of nanoparticles.

According to the materials characterization described in the previous paragraph, we can conclude that in the case of UCA-TP product, an organic–inorganic hybrid gel is produced because of the co-condensation between the silica oligomer and PDMS. In the case of the nanocomposite UCA-TPS, a similar co-condensation process takes place, extending moreover to the silica nanoparticles added to the starting sol, which are perfectly integrated in the silica polymer network.

We also demonstrate that, for the two formulations under study, the *n*-octylamine creates hydrogen bonds with the silica, and is partially removed after air drying of the xerogels. The surfactant prevents gels cracking by reducing the surface tension and by coarsening the pore size of gel network. *n*-octylamine also acts a basic catalyst of the sol–gel transition, creating a polymer network composed of silica particles of nearly uniform size by an aggregative growth mechanism.

Application on Stone Surfaces and Characterization. Uptake of the UCA products (0.17 and 0.22% w/w for UCATP and UCATPS, respectively) was significantly higher than that corresponding to the BS290 (0.06% w/w). Dry matter values obtained were again almost the same for the two UCA materials (around 0.10% w/w). However, in the case of BS290, dry matter was significantly lower (0.03% w/w), its evaporated mass being around 50% because of its high solvent content. This result suggests that BS290 only creates a film on the stone surface but does not penetrate into the pore structure of the stone.

Table 4 shows water droplet static and dynamic contact angle (CA) for the untreated surfaces of stone samples and their treated counterparts. The untreated stone is a hydrophilic material, as confirmed by the low value of its static CA (14°). The dynamic CA could not be measured in the untreated sample because the water droplet was absorbed.

Table 4. Static CA Values and Their Corresponding Advancing and Receding CA for the Stones Treated

product	static CA (deg)	advancing CA (deg)	receding CA (deg)	hysteresis (deg)
untreated	14 ± 2			
BS290	131 ± 11	136 ± 4	114 ± 1	22 ± 3
UCA-TP	140 ± 3	146 ± 1	132 ± 2	13 ± 1
UCA-TPS	149 ± 2	150 ± 1	143 ± 1	7 ± 1

After the application of the products under study a substantial increase was found in the static CA, to 131° on the surface treated with the commercial product and to 140° on the UCA-TP surface, showing that these two products give rise to hydrophobic behavior. It is well-known that the hydrophobic behavior produced by BS290 and UCA-TP is caused by the organic component integrated into their silica gel network, which promotes the reduction of surface energy. In the literature similar behaviors are reported in hybrid gels containing organic components such as PDMS.[15,36]

In the case of the nanocomposite developed in our laboratory, the water droplet static CA was even higher (149°). This highlights how the surface roughness, created by the silica particles, induces superhydrophobicity on the stone surface.

Regarding the hysteresis between advancing CA and receding CA, this parameter is greatly modified, from 22° (BS290) and 13° (UCA-TP, material without particles) to 7° (UCA-TPS, composite including particles). This demonstrates that the surface treated with the nanocomposite achieved water repellence since hysteresis controls the drop movement and in consequence the repellence phenomena.[3]

The values of these two parameters (CA of around 150° and hysteresis of <10°) suggests that superhydrophobicity is induced on the stone surface treated with the polymer–particle nanocomposite synthesized in our laboratory. To confirm this behavior, we carried out several tests. Figure 5 shows a photograph of water droplets on a UCA-TPS treated stone surface. In the case of the stone treated with UCA-TP, droplets display similar contact angle values (the photograph was not included). For comparison, an image of water droplets on an untreated stone surface is also included in the figure. The photographs show that the droplets display high contact angles on the stone surface treated with the nanocomposite, whereas the untreated stone is a hydrophilic material.

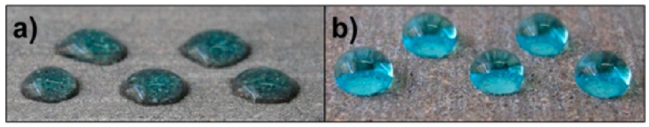

Figure 5. Optical photographs of water droplets on (a) an untreated stone surface and (b) an UCA-TPS stone surface. A small amount of methylene blue dye was dissolved in water for illustration purposes.

Figure 6 shows some of the recorded photograms taken in the water adhesion test. The complete video is shown in Supporting Information (video S1). In the case of the untreated surface, adhesion between water and substrate is clearly observed, as expected for a hydrophilic surface. In contrast, the droplet does not show any tendency to adhere to the UCA-TPS-treated surface. The drop adheres to the tip of the needle and does not move when the stone surface is moved from left to right, as clearly observed in Figure 6 and Video S1 in the

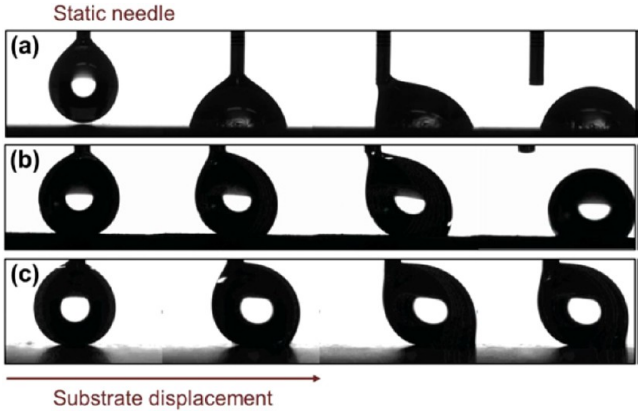

Figure 6. Captured video images of a sessile water droplet on a moving stone surface; (a) untreated surface, (b) surface treated with UCA-TP, (c) surface treated with UCA-TPS.

Supporting Information. The droplet also presents adhesion to the UCA-TP surface in spite of the high value of the CA. This feature confirms that UCA-TP produces a high CA for the stone surface, but it does not induce superhydrophobicity.

In the repellence test, we observe the rapid rolling motion of the droplets on the stone specimen treated with UCA-TPS: they do not stick on the stone surface. This confirms that the nanocomposite synthesized in our laboratory gives water repellent properties to the stone. The video of this experiment can be found in Video S2 in the Supporting Information.

The UCA-TPS stone sample and its untreated counterpart were soaked with running cold water from a tap (see Video S3 in the Supporting Information). As observed, the untreated stone was evidently wet whereas the UCATPS material remained completely dry after the test, demonstrating that water does not penetrate in the treated stone sample.

We also carried out a capillary water absorption test. Total water uptake (TWU) values obtained are shown in Supporting Information (Table S1). The three products under study reduced the water uptake values to almost zero, confirming that water does not penetrate into the treated stone specimens after immersion for 48 h.

It is concluded that all the experiments carried out confirm the superhydrophobic behavior of the stone treated with the UCA-TPS coating material. Since there are explanations in the literature of how this behavior is a consequence of the combination of roughness and the reduction of the surface energy,[9,10,37] we examined the morphology of the coatings in order to confirm the role played by the nanocomposite coating in producing roughness. Figure 7 shows AFM and SEM images obtained for the stone surfaces under study. To clarify this discussion, we also included the pictures of droplets obtained on these surfaces, in an inset.

The surface topography indicated by the AFM images agrees very well with that from the SEM images. In addition, the morphology of the surfaces obtained (AFM and SEM) perfectly matches the CA results obtained, as explained in the following paragraphs.

The untreated stone surface presents a random roughness associated with the heterogeneity of the stone. The morphology of the stone is practically unmodified after the treatment with the commercial product. It suggests that BS290 is not capable of covering the underlying substrate.[38]

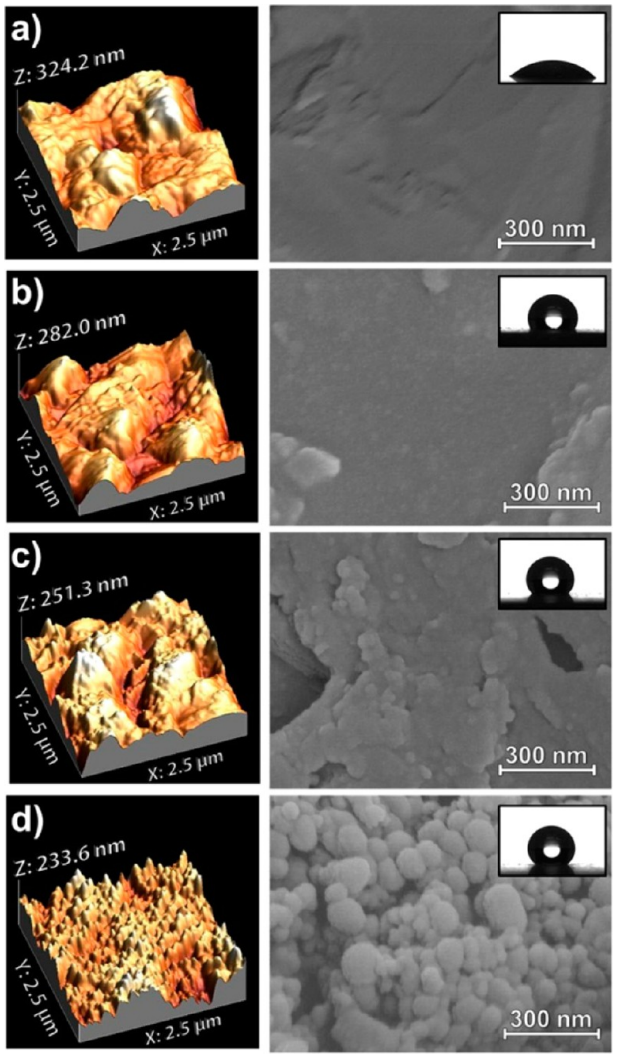

Figure 7. AFM 2D and 3D topography images and SEM images of the surface of the untreated stone and its treated counterparts: (a) untreated, (b) BS290, (c) UCA-TP, (d) UCA-TPS.

In the case of the stone surface with UCA-TP coating, we can observe some modification of the surface. As previously discussed in the TEM photographs (Figure 4), the *n*-octylamine creates a silica gel composed of uniform particles that are perfectly observed on the stone surface visualized by SEM. We can even measure the size of the particles, and find the diameter to be around 60 nm, as previously reported.[13] Nevertheless, the distribution of these particles on the surface is random and they are not very densely packed.

For the nanocomposite material (UCA-TPS), the morphology of the coating is substantially different. Specifically, the OX-50 commercial silica particles integrated in the starting sol are aggregated with the silica particles created during sol−gel transition. Thus, larger aggregates of particles are created, in good agreement with the behavior observed by TEM and discussed earlier in this paper (see Figure 4). Thus, we can clearly observe a coating on the stone surface composed of densely packed uniform particles of around 100−120 nm. We think that the formation of this close-packed coating on the stone surface is the key factor that induces the property of superhydrophobicity. The UCA-TPS surface could be consid-

ered a Cassie–Baxter nonwettable surface with air pockets trapped in between the aggregates of particles.[38]

Figure 8 gives the size distribution for the roughness of the stone surfaces under study, and the RMS roughness obtained.

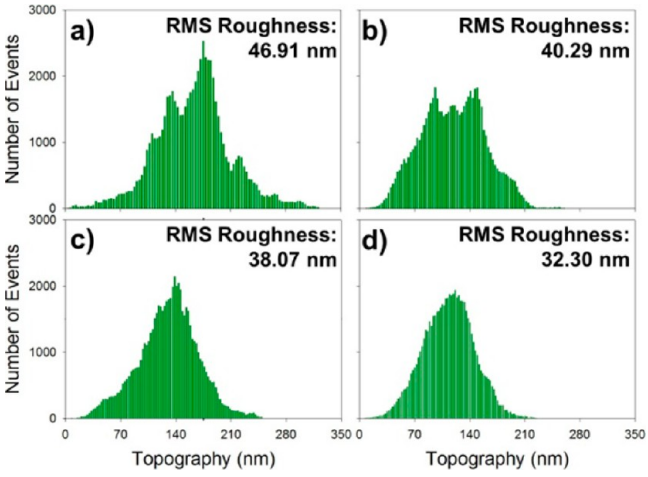

Figure 8. Size distribution of the roughness on the stone surfaces under study: (a) untreated, (b) BS290, (c) UCA-TP, (d) UCA-TPS.

The results included in this last figure show two important features: (1) the average roughness is reduced after the application of all the products under study, suggesting that after application to the stone, all the coatings tend to fill the grooves present in the untreated stone; the greatest reduction in original roughness corresponds to the nanocomposite coating (UCA-TPS). (2) Uniformity of roughness is also increased after application of all the coatings, and again the greatest increase in uniformity is seen in the surface coated by the UCA-TPS composite.

Figure 9 presents the AFM 2D profiles for the surfaces under study. It should be noted that the spacing between the textural peaks of the roughness is important for the trapping of air pockets.[5,39] The greater the distance between peaks (i.e., the spacing), the easier it is for water to penetrate more deeply into the grooves and become more firmly attached to the surface.

From the profiles obtained (see Figure 9), it can be seen that the superhydrophobic UCA-TPS surface presents significantly less distance between roughness peaks (i.e., the pitch) than those corresponding to the other coatings under study, with fairly uniform values of around 100 nm. The other coatings and the untreated surfaces show more heterogeneous pitch values ranging from 1000 to 500 nm. These results suggest that the water droplet will be less able to penetrate the pitch profile created by the UCA-TPS coating on the stone surface; hence the contact area between droplet and surface will be minimized, resulting in a high static contact angle and low adhesion.[39] In the other surfaces evaluated, their larger pitch value indicates a lower contact area between surface and coating, so water can more easily penetrate the grooves and valleys. This produces a decrease in the contact angle values and an increase in contact angle hysteresis and in adhesion. For comparison, Figure 10 illustrates the water droplet contact with an untreated stone sample and a stone coated with UCA-TPS.

An important limitation of these products for their application is to produce changes in the color of the building material treated. Therefore, total color difference values (ΔE^*) of the stone induced by the products were measured and the

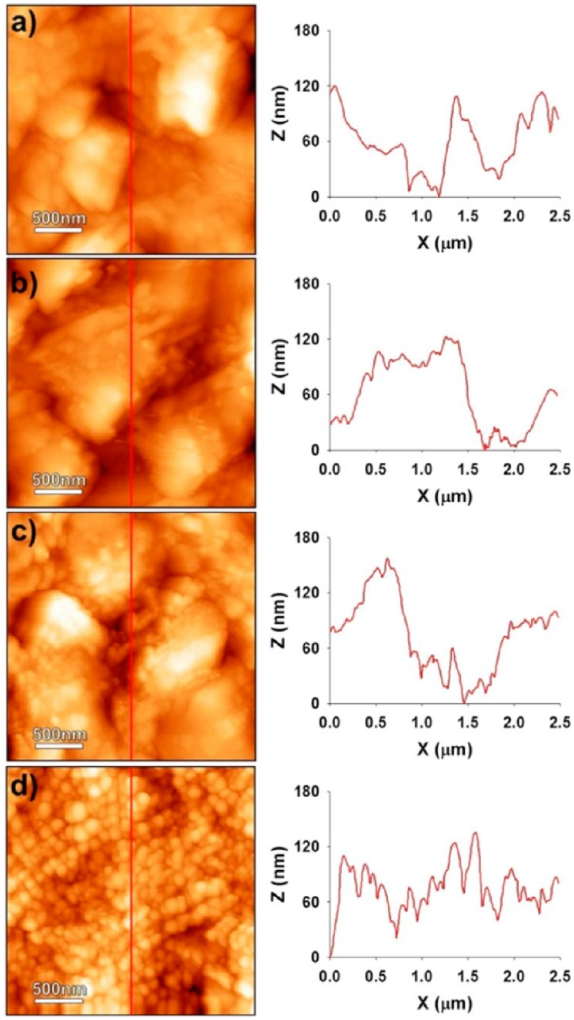

Figure 9. Roughness 2D profiles of the surface of the untreated stone and its treated counterparts. Red lines show the path followed to obtain the profile: (a) untreated, (b) BS290, (c) UCA-TP, (d) UCA-TPS.

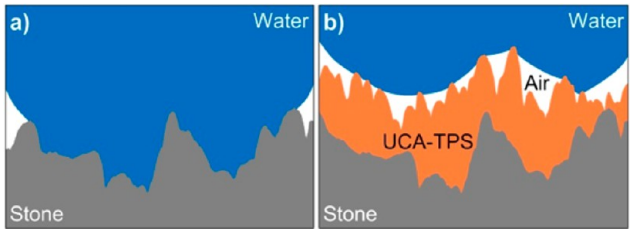

Figure 10. Illustration of a water droplet in contact with the stone surface: (a) untreated, (b) treated with UCA-TPS.

results can be found in the Supporting Information (see Table S1). All the products produced some change in color but close to the generally accepted threshold value $\Delta E^* \leq 3$.[25]

One drawback of existing hydrophobic products applied on the surfaces of buildings and structures is that their effectiveness tends to decrease over time, during long-term use. This decrease can be minimized if the product penetrates deeply into the pore structure of the building material, thus achieving good product-substrate adhesion. We investigated the depth of penetration of the products under study in cross sections of the

untreated and treated stone specimens. Figure 11 shows images of these cross-sections after immersion in water.

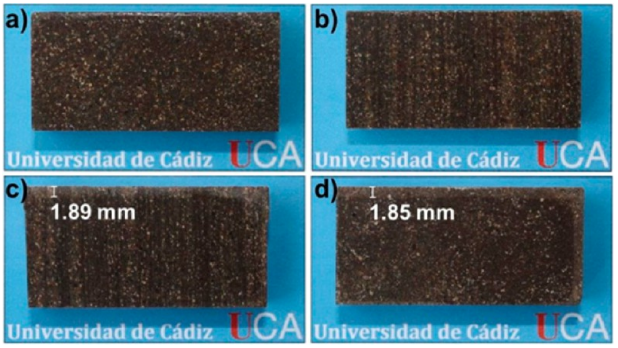

Figure 11. Wet cross sections of the untreated stone sample and its treated counterparts: (a) untreated, (b) BS290, (c) UCA-TP, (d) UCA-TPS.

The pictures show that the two UCA products do penetrate into the stone pore structure because a dry zone to a depth of 1.9 mm is clearly observed. In the case of the BS290 stone and the untreated specimen, the cross-section was completely wet from the surface down. This test confirms that the commercial product produces only a thin film on the stone surface and it does not penetrate into its porous structure.

All the positive results discussed in the preceding paragraph suggest the material synthesized in our laboratory has an immediate practical application. The novel product will be commercialized under an exploitation patent.[40]

CONCLUSIONS

We have developed a simple and low-cost synthesis route for creating superhydrophobic surfaces on stones and other building materials. Because the synthesis is a simple one-step process, it meets the operational requirement for straightforward, single-stage outdoor application, and it can easily be adapted for mass-production. The starting sol can be applied on the building material by various simple procedures, such as spraying or brushing, and there is no need for any additional operation, like heating. Another environmental advantage is that no volatile organic components are employed in this synthesis route.

From our investigation of the texture of this nanocomposite, we conclude that the addition of silica nanoparticles is a key factor in imparting the superhydrophobic property to the material. These nanoparticles produce a densely packed coating in which the air is trapped. Thus, water droplets cannot penetrate into the coating, and the contact area between droplet and surface is significantly minimized. In addition, the organic component reduces the surface free energy. This results in a high static contact angle (~150°) and low hysteresis values (~7°). The surfactant plays a valuable role whereby it acts to coarsen the pore gel network, thus preventing cracking during drying. The surfactant also acts as a catalyst of the sol–gel transition.

Finally, we demonstrate this nanocomposite applied on a building stone produces a homogeneous coating, giving measurable hydrophobic and repellence properties to the stone evaluated. Moreover, the product penetrates well into the pore structure of the stone; it achieves the required adhesion; and it preserves the aesthetic qualities of the substrate.

ASSOCIATED CONTENT

Supporting Information

TEM image of the commercial OX-50 particles; videos of the water adhesion, repellence and soaking tests; and a table including water uptake, color and penetration depth data. This material is available free of charge via the Internet at http://pubs.acs.org.

AUTHOR INFORMATION

Corresponding Author

*E-mail: mariajesus.mosquera@uca.es. Fax: +34-956016471. Tel: +34-956016331.

Notes

The authors declare no competing financial interest.

ACKNOWLEDGMENTS

We are grateful for financial support from the Spanish Government/FEDER-EU (Project MAT2010-16206 and Project Geometrización Petrea, Innpacto subprogram), and from the Government of Andalusia (project TEP-6386 and Group TEP-243). D.S.F. thanks the Spanish Government for his predoctoral grant (BES-2011-045657) associated with the project MAT2010-16206.

REFERENCES

(1) Erbil, H. Y.; Demirel, A. L.; Avci, Y.; Mert, O. *Science* **2003**, *299*, 1377–1380.
(2) Gao, L.; McCarthy, T. J. *Langmuir* **2009**, *25*, 14105–14115.
(3) Gao, L.; McCarthy, T. J. *Langmuir* **2006**, *22*, 5998–6000.
(4) Barthlott, W.; Neinhuis, C. *Planta* **1997**, *202*, 1–8.
(5) Öner, D.; McCarthy, T. J. *Langmuir* **2000**, *16*, 7777–7782.
(6) McHale, G.; Aqil, S.; Shirtcliffe, N. J.; Newton, M. I.; Erbil, H. Y. *Langmuir* **2005**, *21*, 11053–11060.
(7) Hikita, M.; Tanaka, K.; Nakamura, T.; Kajiyama, T.; Takahara, A. *Langmuir* **2005**, *21*, 7299–7302.
(8) Latthe, S. S.; Imai, H.; Ganesan, V.; Rao, A. V. *Microporous Mesoporous Mater.* **2010**, *130*, 115–121.
(9) Manoudis, P. N.; Karapanagiotis, I.; Tsakalof, A.; Zuburtikudis, I.; Panayiotou, C. *Langmuir* **2008**, *24*, 11225–11232.
(10) Karapanagiotis, I.; Manoudis, P. N.; Savva, A.; Panayiotou, C. *Surf. Interface Anal.* **2012**, *44*, 870–875.
(11) de Ferri, L.; Lottici, P. P.; Lorenzi, A.; Montenero, A.; Salvioli-Mariani, E. *J. Cult. Herit.* **2011**, *12*, 356–363.
(12) Mosquera, M. J.; de los Santos, D. M.; Montes, A.; Valdez-Castro, L. *Langmuir* **2008**, *24*, 2772–2778.
(13) Illescas, J. F.; Mosquera, M. J. *Appl. Mater. Interfaces* **2012**, *4*, 4259–4269.
(14) Mosquera, M. J.; de los Santos, D. M.; Rivas, T. *Langmuir* **2010**, *26*, 6737–6745.
(15) Illescas, J. F.; Mosquera, M. J. *J. Phys. Chem. C.* **2011**, *115*, 14624–14634.
(16) Pinho, L.; Mosquera, M. J. *J. Phys. Chem. C* **2011**, *115*, 22851–22862.
(17) Pinho, L.; Hernandez-Garrido, J. C.; Calvino, J. J.; Mosquera, M. J. *Phys. Chem. Chem. Phys.* **2013**, *15*, 2800–2808.
(18) Pinho, L.; Mosquera, M. J. *Appl. Catal. B* **2013**, *134–135*, 205–221.
(19) Pinho, L.; Elhaddad, F.; Facio, D. S.; Mosquera, M. J. *Appl. Surf. Sci.* **2013**, *275*, 389–396.
(20) Mosquera, M. J.; Montes, A.; de los Santos, M. D. U.S. Patent. no. US 2008/0209847 A1, September 4, 2012.
(21) Mosquera, M. J.; Pinho, L.; Spanish Patent no. P201100741. Priority date: June 24, 2011.
(22) Mosquera, M. J.; Illescas, J. F.; Spanish Patent No. P201100339. Priority date: March 21, 2011.

(23) Mirgorodskaya, A. B.; Kudryavtseva, L. A.; Zuev, Y. F.; Archipov, V. P.; Idiyatullin, Z.Sh. *Mendeleev Commun.* **1999**, *5*, 171−212.
(24) *UNE-EN 1925; Natural Stone Test Methods. Determination of Water Absorption Coefficient by Capillarity*; AENOR: Madrid, Spain, 1999.
(25) Berns, R. S. *Billmeyer and Saltzman's Principles of Color Technology*; Wiley-Interscience: New York, 2000.
(26) Mosquera, M. J.; de los Santos, D. M.; Valdez-Castro, L.; Esquivias, L. *J. Non-Cryst. Solids* **2008**, *354*, 645−650.
(27) Mackenzie, J. D.; Chung, Y. J.; Hu, Y. *J. Non-Cryst. Solids* **1992**, *147&148*, 271−279.
(28) Kruk, M.; Jaroniec, M. *Chem. Mater.* **2001**, *13*, 3169−3183.
(29) Kruk, M.; Jaroniec, M. *Langmuir* **1997**, *13*, 6267−6273.
(30) Barret, E. P.; Joyner, L. G.; Halenda, P. P. *J. Am. Chem. Soc.* **1951**, *73*, 373.
(31) Mosquera, M. J.; de los Santos, D. M.; Rivas, T.; Sanmartin, P.; Silva, B. *J. Nano R.* **2009**, *8*, 1−12.
(32) Tanev, P. T.; Pinnavaia, T. J. *Chem. Mater.* **1996**, *8*, 2068−2079.
(33) Orcel, G.; Hench, L. L.; Artaki, I.; Jonas, J.; Zerda, T. W. *J. Non-Cryst. Solids* **1988**, *105*, 223−231.
(34) Bogush, G. H.; Zukoski, C. F., IV *J. Colloid Interface Sci.* **1991**, *142*, 1−18.
(35) Bogush, G. H.; Zukoski, C. F., IV *J. Colloid Interface Sci.* **1991**, *142*, 19−34.
(36) Wu, Y. L.; Chen, Z.; Zeng, X. T. *Appl. Surf. Sci.* **2008**, *254*, 6952−6958.
(37) Chen, W.; Fadeev, A. Y.; Hsieh, M. C.; Öner, D.; Youngblood, J.; McCarthy, T. J. *Langmuir* **1999**, *15*, 3395−3399.
(38) Xu, L.; Karunakaran, R. G.; Guo, J.; Yang, S. *Appl. Mater. Interfaces* **2012**, *4*, 1118−1125.
(39) Bhushan, B.; Her, E. K. *Langmuir* **2010**, *26*, 8207−8217.
(40) Mosquera, M. J.; Illescas, J. F.; Facio, D. S. Spanish Patent no. P201200152. Priority data: February 16, 2012.